THERMO-MECHANICAL BEHAVIOUR OF SINGLE-PLY TRIAXIAL WEAVE CARBON FIBRE REINFORCED PLASTIC

Ahmad Kueh, Omer Soykasap, and Sergio Pellegrino

Department of Engineering, University of Cambridge, Trumpington Street, Cambridge, CB2 1PZ, U.K.

ABSTRACT

This paper is concerned with the thermo-mechanical behaviour of composite structures made from a single ply of Triaxial Woven Fabric (TWF) cured with epoxy resin. Seemingly unpredictable behaviour has been recently reported for this material. We present a series of carefully obtained experimental results, which correlate accurately with simple micro-mechanical models.

1. INTRODUCTION

This paper is concerned with the thermo-mechanical behaviour of composite structures made from a single ply of Triaxial Weave Fabric (TWF) cured with epoxy resin. A particular attraction of this material is that it is mechanically quasi-isotropic on a macroscopic scale, and so it can be used to construct ultra-thin structural elements from a single ply. This feature makes it particularly attractive to designers of spacecraft antennas and the next generation of low cost deployable structures.

However, when one looks carefully, the behaviour of this material is rather more subtle than standard composite laminates, which are made by stacking many plies, and this has resulted in some recent studies reporting seemingly unexpected behaviour, leading to the widespread impression that TWF is unpredictable. We believe that this is not the case, and in this paper we present a series of carefully obtained experimental results which are correlated with relatively simple micro-mechanical models. These models capture the experimentally observed behaviour of single-ply TWF, and thus can be used to explain the apparent anomalies that have been reported. Moreover, the mechanical properties of single-ply TWF are predicted with an accuracy of around 10% by these models. A thermo-mechanical instability has been observed, and is discussed in the paper.

The particular type of TWF that is investigated in this paper is SK-802, made by Sakase-Adtech Ltd., Japan. This fabric consists of 1000 filament bundles of T-300 carbon fibre woven in the "basic weave" pattern shown in Fig. 1. The weave consists of a set of fill yarns, horizontal in the figure, and two sets of warp yarns, at angles of $+60^\circ$ and -60°, forming large hexagonal holes. The fill-direction will be denoted as 0-direction in this paper, and we will be interested also in the properties of the material in the direction perpendicular to the fill, which will be denoted as the 90-direction. SK-802 has a dry mass of 75 g/m^2 and a thickness of 0.14 mm.

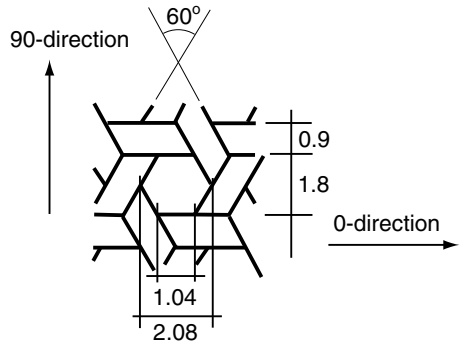

Figure 1. Dimensions, in mm, of unit cell of SK-802.

Four specific issues are investigated in the paper, as follows.

(i) Edge effects, which are most noticeable when TWF is loaded at 90 degrees to one set of tows.

(ii) Crimp angle effects, which result in (a) lower stiffness at small strains and (b) a variation in the Poisson's ratios of TWF as the applied strain increases. These effects are fully captured by means of a three-dimensional, geometrically non-linear model of TWF.

(iii) Bending stiffness and ultimate bending curvature.

(iv) Thermo-mechanical coupling between bending and twisting, which in plates with an aspect ratio of around one leads to thermal buckling.

2. MATERIALS

TWF is laid up between two layers of semi-solid resin film, on a release paper. The resin used is Hexcel 913, from Hexcel Composites, which has a temperature cure cycle of 125°C. The lay-up is then heated to allow the resin to first melt and then flow into the fabric; it is then put in a refrigerator until the resin hardens, and then the release paper is removed. Finally the lay-up is cured in an autoclave. The material properties of the yarns and the matrix are listed in Table 1.

Table 1. Properties of T-300 carbon fibres and Hexcel 913 epoxy

Property	T-300	913
Density (kg/m^3)	1,760	1,230
Elastic Modulus, E_1 (MPa)	230,000	3,320
Elastic Modulus, E_2 (MPa)	14,000	
Shear Modulus, G_{12} (MPa)	8,960	1,210
Poisson's ratio, ν_{12}	0.2	0.41
Poisson's ratio, ν_{21}	0.01	
Tensile Strength (MPa)	3,530	65.5
Maximum strain (%)	1.5	–
CTE	-0.41×10^{-6}	$\approx 80 \times 10^{-6}$

Figure 2 shows five micrographs of closely-spaced consecutive sections of a particular tow; the direction of viewing is shown with an arrow. These micrographs can be used to determine the properties of a beam approximately equivalent to this tow.

In the present study, the cross-section of each tow has been modelled as a rectangle with height equal to half the thickness of the cured ply, measured from the micrographs, and found to have an average value of 0.078 mm. The width of the rectangle is set at 0.947 mm, in order to achieve an area equal to the average measured cross-sectional area of the tow. The measured volume fraction of fibres is $V_f = 0.52$.

The tow is modelled as a linear-elastic, transversally isotropic material whose properties are determined as follows [1].

The longitudinal extensional modulus, E_1, is obtained from the rule of mixtures

$$E_1 = E_{1f}V_f + E_m(1 - V_f) = 121,194 \text{ MPa} \qquad (1)$$

The Poisson's ratio is also found from the rule of mixtures

$$\nu_{12} = \nu_{13} = \nu_{12f}V_f + \nu_m V_f = 0.30 \qquad (2)$$

The transverse extensional modulus is found from the Halpin-Tsai semi-empirical relation

$$E_2 = E_3 = E_m \frac{1 + \xi_1 \eta_1 V_f}{1 - \eta_1 V_f} \qquad (3)$$

where

$$\eta_1 = \frac{E_{2f} - E_m}{E_{2f} + \xi_1 E_m} \qquad (4)$$

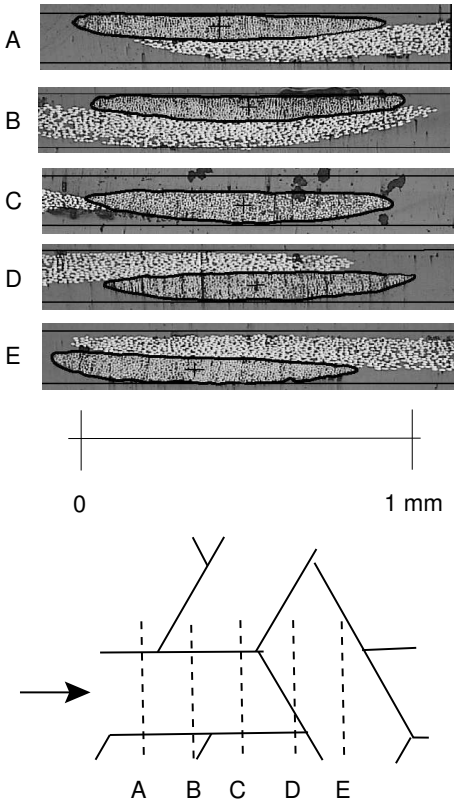

Figure 2. Sections of a tow.

and the value $\xi_1 = 2.0$ has been chosen. This gives $E_2 = 7,081$ MPa.

The shear modulus $G_{12} = G_{13}$ is found from the Halpin-Tsai semi-empirical relation (with the reinforcing efficiency factor set to 1 as suggested in [1])

$$\begin{aligned} G_{12} = G_{13} &= G_m \frac{(G_{12f} + G_m) + V_f(G_{12f} - G_m)}{(G_{12f} + G_m) - V_f(G_{12f} - G_m)} \\ &= 2,879 \text{ M}Pa \end{aligned} \qquad (5)$$

The derivation of the in-plane shear modulus G_{23} follows [2]. It is rather lengthy and is not shown here; the outcome is $G_{23} = 2,859$ MPa. Then, ν_{23} is computed from

$$G_{23} = \frac{E_2}{2(1 + \nu_{23})} \qquad (6)$$

3. IN-PLANE PROPERTIES

3.1. Edge Effects

It is important to realize that the aspect ratio of the specimen used in a tension test is likely to affect the measurements. Understanding these effects is important to decide which properties should be used in the analysis of actual

structures made of TWF, a computational study of edge effects was carried out.

A series of 110 mm long strips of TWF were investigated by finite-element analysis (details are given in Section 3.3). This particular length was chosen to match the length of the specimen that would be tested, and the direction of loading was set either in the 0-direction, or in the 90-direction. Each TWF strip was modelled as a two-dimensional lattice of beams with rectangular cross-section, with fully-rigid connections at each cross-over point and fully built-in end conditions.

Figure 3 shows plots of the stiffness predicted by this model. Note that there is a clear increasing trend for the stiffness S_{90}, whereas the stiffness S_0 is almost constant. The plots show that S_{90} can be expected to be about 10% lower than S_0 for a specimen with a width to length ratio of about 0.25 (as in the tests described in Section 3.2).

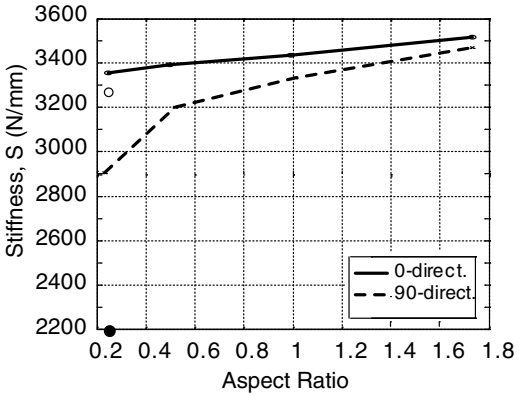

Figure 3. Variation of axial stiffness with aspect ratio (width/length) of tensile specimens, and two sets of experimental measurements.

3.2. Measurements of In-Plane Stiffness

The tension tests were carried out with an Instron 5578 materials testing machine, fitted with a 2 kN load cell. The longitudinal and transverse extensions of the specimen over gauge lengths of 50 mm and 10 mm, respectively, were measured with Epsilon LE-01 and LE-05 laser extensometers. The average strains were determined from these measurements.

The tension test specimens were cut with straight edges and sandwiched at the ends between aluminium plates, Figure 4 shows the details. In most tests the maximum average strain was limited to 0.6%, i.e. well below failure as the main aim of these tests is to characterize the stiffness of single-ply TWF, not their strength.

Figure 5 shows two sample sets of measurements. Note that the relationship between force per unit width and strain is almost linear in the direction of loading, but approximately bilinear in the transverse direction.

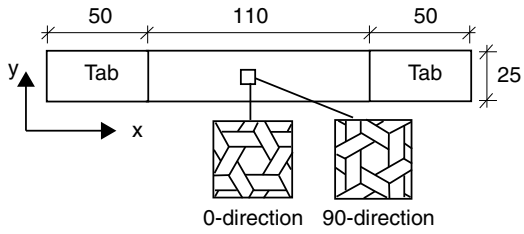

Figure 4. Specimens used in the tension tests (dimensions in mm).

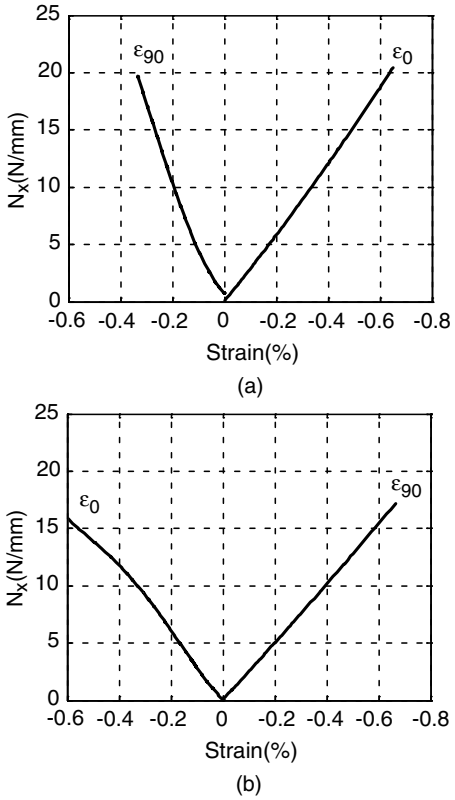

Figure 5. Sample tension test measurements for (a) 0-direction and (b) 90-direction.

Plotting the longitudinal strain vs. the transverse strain for the two types of specimen, Fig. 6, shows that the relationship is approximately bi-linear. The change in slope occurs at a strain of about 0.32%, and the slope decreases for a 0-direction specimen, whereas it increases for a 90-direction specimen.

The results of the tests are summarized in Table 2. Note that in the table two values have been included for the Poisson's ratio, one for longitudinal strains below 0.32% and one above.

The average measured stiffnesses have been plotted in Fig. 3, with a circle for S_0 and a solid dot for S_{90}. Note that the simple 2D prediction for S_0 is very accurate, but the prediction for S_{90} is about 25% too high.

3.3. Finite-Element Simulations

Two types of finite element models were used. The simple 2D lattice model employed in Section 3.2 consisted of three-node quadratic Timoshenko beams, using element B22 in ABAQUS version 6.5. A more refined, 3D model of half of the tension test specimen was also set up to capture the geometrically non-linear effects due to the waviness of the tows. For this model, the elements are 3-node quadratic beams in 3D, B32. The boundary

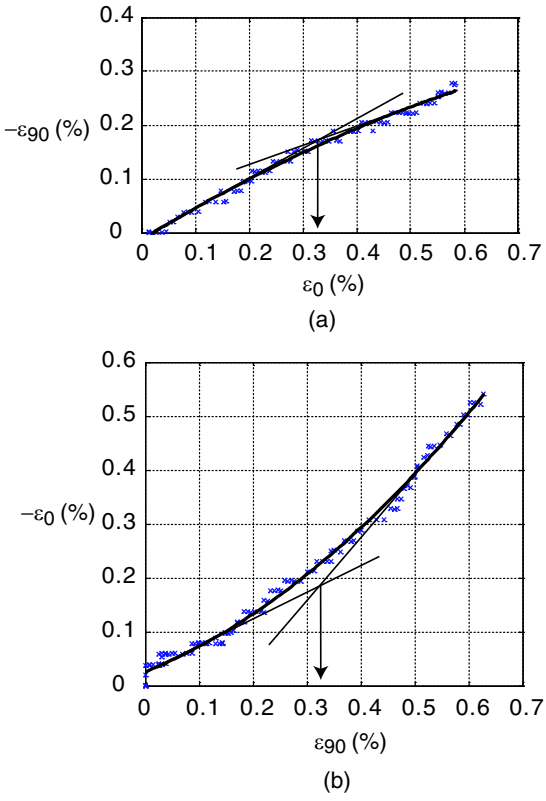

Figure 6. Longitudinal vs. transverse strains for (a) 0-direction and (b) 90-direction tests.

Table 2. Measured in-plane stiffnesses and Poisson's ratios

Specimen	**Stiffness** (N/mm)		**Poisson's ratios**	
	S_0	S_{90}	$\nu_{0,90}$	$\nu_{90,0}$
1	3,364	2,322	0.605/0.375	0.732/1.059
2	3,196	2,256	0.520/0.438	0.774/1.095
3	3,120	2,095	0.556/0.367	0.713/1.159
4	3,211	1,992	0.536/0.439	0.849/0.964
5	3,541	2,170	0.513/0.450	0.582/0.979
6	3,293	-	0.577/0.447	-
7	3,285	-	0.613/0.469	-
Mean	3,287	2,167	0.560/0.426	0.730/1.051

conditions of the 3D models, which allow for symmetry on the mid-plane of the specimen, are shown in Fig. 7.

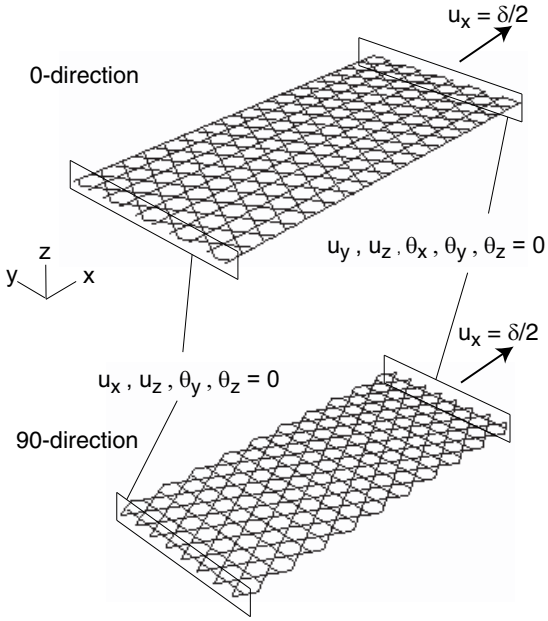

Figure 7. 3D model boundary conditions for two types of specimen.

The transversally isotropic material properties defined in Section 2 were used in the ABAQUS model.

Three different representations of the wavy tows were considered (note that these simulations were done on a shorter model than that tested in the experiments): a half-hexagon, a triangular wave, or a sine wave. The amplitude of all three wave models was 0.039 mm, i.e. a quarter of the thickness of a cured single-ply. A rigid beam connector was used to model the connection between beams at each crossover point; this constraint sets the displacement and rotation of the corresponding nodes to be the same, Fig. 8.

To determine the sensitivity of the predictions to the detailed shape of the wavy beam, plots of load per unit width vs. strain were compared, see Fig. 9. The following observations can be made: the 2D model predicts a

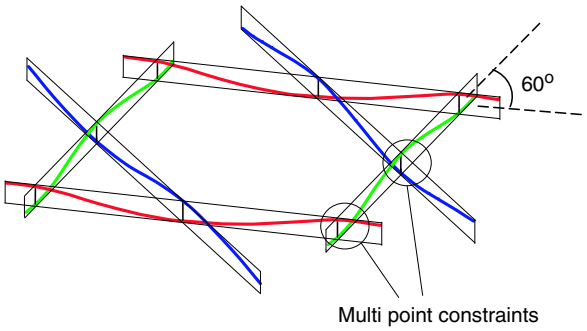

Figure 8. 3D repeating unit.

perfectly linear response; all 3D models predict a bilinear response; neglecting the initial, softer response, the 3D models predict approximately the same stiffness as the 2D model. The stiffness predictions are 3354 N/mm for the 2D model and 3192, 3291, and 3288 N/mm for the 3D models.

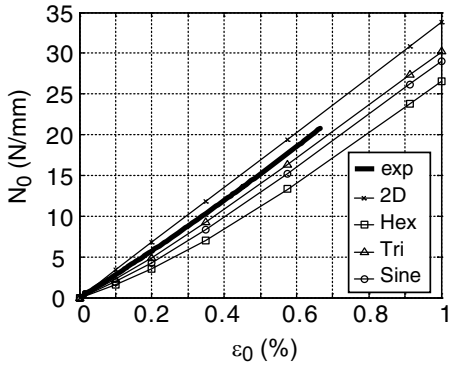

Figure 9. Predictions from finite element models, plus an experimental set of results.

3.4. Simple Analytical Predictions

Simple analytical predictions for the extensional stiffness of single-ply TWF that is pulled in one direction and left unconstrained in the other direction have been derived in [3].

Modelling the tows as a two-dimensional pin-jointed structure, one finds

$$N_0 = \frac{AE}{L}\epsilon_0 \qquad (7)$$

and modelling the tows as shear-stiff beams, one finds

$$N_{90} = \frac{24\sqrt{3}EIA\left(7\,Al^2 + 48\,I\right)}{\left(492\,Al^2I + 5\,A^2l^4 + 1440\,I^2\right)l}\,\varepsilon_{90} \qquad (8)$$

where E, A, and I are the longitudinal modulus, cross-sectional area and second moment of area of the tow about an axis perpendicular to the mid-plane of the TWF. L is the centre-line distance between opposite sides of a hexagon and l is the side length of a hexagon.

Predictions for Poisson's ratios can also be derived from the same two-dimensional models, but they are found to be hopelessly inaccurate.

3.5. Comparison of Results

A comparison between finite element simulations of a particular 0-direction tension test and the actual measurements is shown in Fig. 9. Similar comparisons have been carried out for 90-direction specimens as well. The predicted and measured stiffnesses differ by 3% and 15% in the 0-direction and 90-direction, respectively. The 3D model simulations also predict a similar kind of bilinear transverse response to that observed in the experiments.

Plotting ϵ_y vs. ϵ_x for the 0-direction and 90-direction specimens, Fig. 10, shows the bilinear response very clearly. There is a difference of 5% and 25%, respectively, between the measured Poisson's ratio and those predicted from the 3D model.

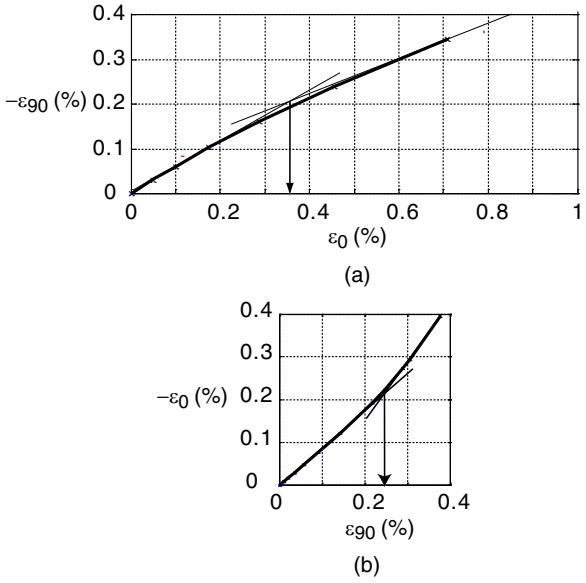

Figure 10. Finite element simulation, with triangular waveform 3D model, of relationship between longitudinal and transverse strain.

Table 3. Comparison of measured and predicted stiffnesses (above transition strain)

	S_0 (N/mm)	S_{90} (N/mm)
Expt. average	3287	2167
FE 2D	3356	2903
FE 3D	3387	1846
Analytical	3313	2892

4. BENDING STIFFNESS AND FAILURE CURVATURE

4.1. Measurements

Figure 11 shows the rig used to measure the bending stiffness. The rig consists of two hollow shafts mounted on gearboxes; one of the gearboxes is mounted on a slider. The specimen is attached to the top ends of the shafts and the gearboxes are turned by equal and opposite amounts. The corresponding moments applied to the specimen are measured by strain-gauges mounted on the surface of the shafts.

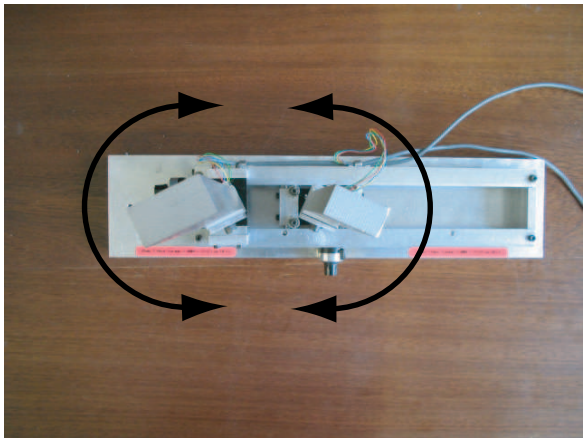

Figure 11. Top view of bending rig (specimen not shown).

Bending tests were carried out on 25×50 mm single-ply TWF strips; both 0-direction and 90-direction specimens were tested. Plots of moment per unit width vs. curvature, obtained from the tests, are shown in Fig. 12. The test results are summarized in Table 4.

An additional set of tests was carried out to determine the minimum radius to which one and two-ply, 0-direction TWF specimens can be folded without damage.

The length of the specimens is $15 \times (\pi \overline{R}_{min} + 30)$ mm, where $\overline{R}_{min}$ is a preliminary estimate of the radius at failure. A specimen is attached to square rods connected to the Instron testing machine, as depicted in Figure 13. The cross-head of the Instron is moved at a rate of 0.1 mm/s, thus gradually bending the specimen. The shape of the

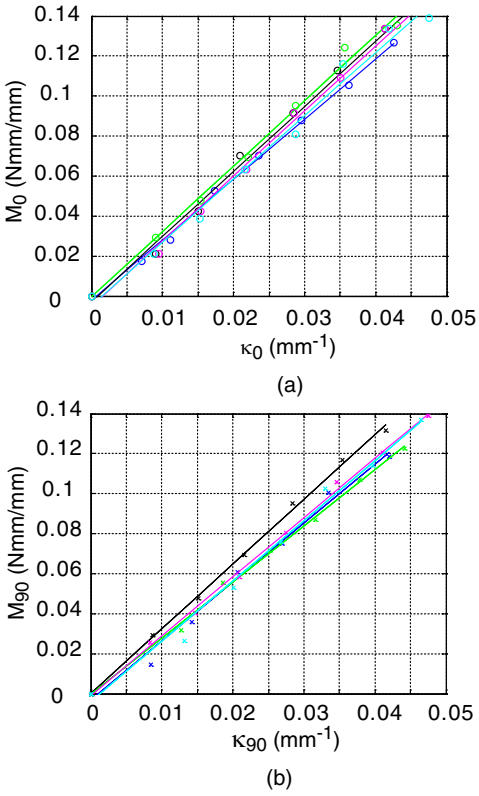

Figure 12. Measurements of moment per unit width vs. curvature.

Table 4. Measured bending stiffnesses

Specimen	**Bending stiffness, D (Nmm)**	
	0-direction	**90-direction**
1	3.013	2.942
2	3.254	3.232
3	3.273	2.800
4	3.250	2.964
5	3.158	3.002
Mean	3.190	2.988

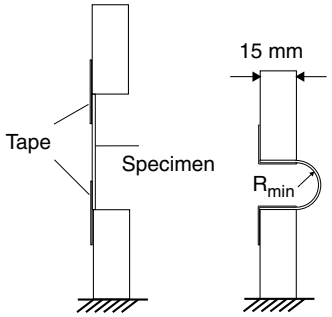

Figure 13. Minimum radius test layout.

Table 5. Measured minimum radii of curvature

Specimen	Minimum radius, R (mm)	
	One ply	Two plies
1	2.24	4.57
2	2.33	4.31
3	2.16	4.31
4	2.16	4.14
Mean	2.22	4.33

specimen during the test is monitored with a digital video camera, until the specimen breaks. At this point, the minimum radius of curvature, R_{min}, is determined from the video image right before the specimen breaks.

The results of these experiments are shown in Table 5. The average failure curvatures, which are required to determine the margin against failure of a folded structure, are 0.45 mm^{-1} and 0.23 mm^{-1} for one-ply and two-ply TWF, respectively.

4.2. Predictions

The bending stiffness of single-ply TWF can be estimated by considering the D_{11} bending stiffness of three plates, each representing one set of tows, with unidirectional fibres at $0°$, $60°$, and $-60°$. The thickness of each plate is equal to the thickness of a single tow. From classical lamination theory, we find $D_{11} = 4.8,\ 0.6,\ 0.6$ Nmm, respectively, for the three plates. Adding these three contributions and dividing by 3, because each set of tows covers only one third of TWF, gives an estimate of 2.00 Nmm for the bending stiffness. It is interesting to compare this simple estimate to the values predicted by the 3D finite element model, which are 2.50 and 2.09 Nmm respectively in the 0-direction and the 90-direction. Both sets of predictions are underestimates of the measured stiffnesses, which are respectively 3.19 and 3.00 Nmm, see Table 4.

R_{min} can be estimated by considering the kinematic curvature-strain relationship for a single tow, from standard beam theory. Hence

$$R_{min} = \frac{t}{2\epsilon_{max}} \tag{9}$$

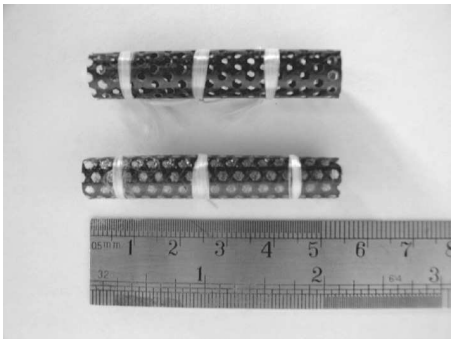

Figure 14. Cylindrical specimens for thermal expansion test.

Table 6. Measured CTE

Measurement	CTE (/°C)	
	0°	90°
1	2.13×10^{-6}	1.59×10^{-6}
2	2.54×10^{-6}	1.64×10^{-6}
3	2.37×10^{-6}	1.60×10^{-6}
Mean	2.35×10^{-6}	1.61×10^{-6}
Std. dev.	0.21×10^{-6}	0.03×10^{-6}
Variance (%)	8.78	1.64

Substituting the tow thickness for t and ϵ_{max} from Table 1 gives, $R_{min} = 2.6$ mm, which is a 17% overestimate of the measured value.

5. COEFFICIENT OF THERMAL EXPANSION

5.1. Specimens

The coefficient of thermal expansion (CTE) of TWF was measured on cylindrical specimens with a diameter of 8 mm and 50 mm long, using a WSK TMA 500 dilatometer. The cylinder axes were either aligned with the 0- or the 90-material directions. The specimens were cured on a 35 mm diameter mandrel, and were then rolled tighter and wrapped with Kevlar cord, see Fig. 14. The test temperature ranged from -150°C to 140°C with a rate 5°C/min.

5.2. Results

Plots of thermal strain versus temperature are shown in Fig. 15; note that the slope of the 0-direction samples is approximately constant, whereas in the 90-direction specimen the slope gradually increases as the temperature increases. The average values of the CTE for the three samples tested are presented in Table 6.

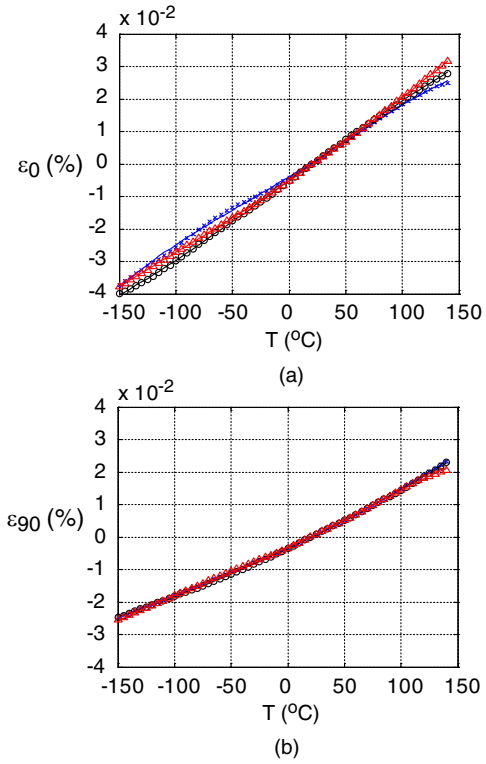

Figure 15. Thermal strain vs temperature for (a) 0-direction and (b) 90-direction.

5.3. Rule-of-Mixture Predictions

A simple estimate of the CTE of TWF can be obtained by estimating the CTE of a composite rod that has a volume fraction V_f of fibres, with modulus E_f and CTE α_f, embedded in a matrix with modulus E_m and CTE α_m. The CTE along the axis of the rod is given by [1]

$$\alpha = \frac{E_{1f}\alpha_f V_f + E_m\alpha_m(1-V_f)}{E_{1f}V_f + E_m(1-V_f)} \qquad (10)$$

The CTE of Hexcel resin 913 is not currently known and so a typical value for unfilled epoxy resins of $80 \times 10^{-6}\,/^{\circ}\mathrm{C}$ will be used. Hence, substituting the values in Table 1 we obtain

$$\alpha = \frac{230000\,(-0.41)\,0.52 + 3320\,(80)\,0.48}{230000 \times 0.52 + 3320 \times 0.48} \times 10^{-6} = 0.65 \times 10^{-6}\,/^{\circ}\mathrm{C}$$

This value is only 27% of the measured value in the 0-direction. The discrepancy may be explained by the CTE of the resin being larger, and the effective modulus of the wavy fibres in the in-plane direction being less than the full value, and possibly also the particular specimens being more resin rich.

To explain the difference between the CTE of TWF in the 0-direction and the 90-direction the 3D wavy-fibre model is required.

6. MEASUREMENT OF THERMAL DISTORTIONS

6.1. Experimental technique

The thermal distortion of one-ply triaxial weave material was measured using the photogrammetry software Photomodeler Pro 5.2.2. Specimens with two different widths, see Fig. 16, were hung inside a thermal chamber, and were heated from 20°C to 170°C at a rate of 3°C/min. Figure 16 shows a photo of a specimen inside the chamber. Both 0- and 90-direction specimens were tested. The temperature inside the chamber was measured with a thermocouple placed close to the specimen. An invar bar was placed next to the specimen, and was used as a reference.

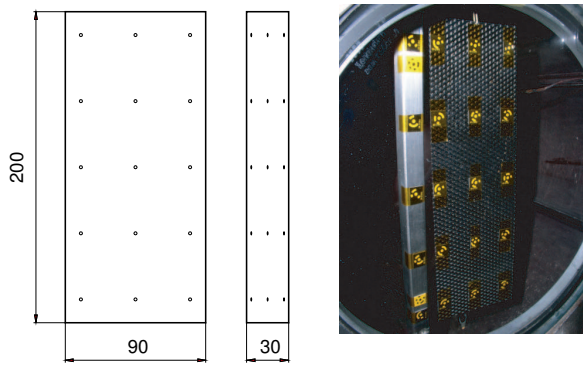

Figure 16. Specimen sizes and location of target points for thermal distortion tests (dimensions in mm).

6.2. Results

All 90 mm wide specimens were cut from the same sheet of TWF, which had been sandwiched between two steel plates for curing. This sheet had an even distribution of resin on both sides. The 60 mm wide and 30 mm wide specimens were cut from a different sheet, which had been cured with only one steel plate, yielding a resin rich, rough surface of one side.

All measurements have a precision of 0.01 mm in each direction. For the 90 mm wide specimens, the maximum out of plane displacement due to thermal loading is 1.2 mm for 90-direction specimens and 2 mm for 0-direction specimens. For the 30 mm wide specimens, the maximum out of plane displacement due to thermal loading is 6.7 mm for 90-direction specimens and 11.2 mm for 0-direction specimens.

It is concluded that relatively significant thermal distortions occur, and are more severe in the narrower specimen.

6.3. Curvature-Temperature Relationship

In order to measure the variation with temperature of the curvature of the specimens, quadratic and cubic polynomials were fitted to the measured points, along the horizontal and vertical directions, respectively. To avoid edge effects, only the points in the central region of the specimens were considered.

Figure 17 shows the variation with temperature of the curvature changes in the 0-direction and the 90-direction, for specimens with two different material orientations. The first thing to note is that the curvature-temperature relationships are non-linear. Second, the two curvatures are in competition with one another, but cannot both grow large as this would require the mid-plane of the structure to stretch. So, from a certain point onwards one curvature decreases to approximately zero while the other curvature grows. Third, the curvature that ultimately grows, at larger temperatures, is along the shorter side length for both types of specimen.

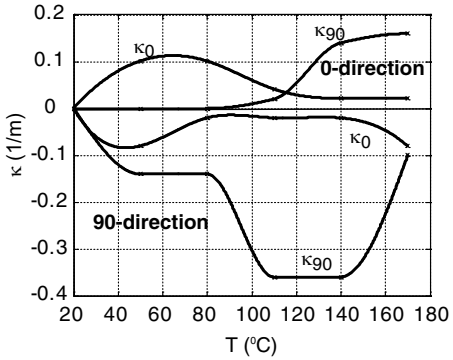

Figure 17. Curvature versus temperature relationship for 90 mm wide specimen.

For the 90 mm wide specimens, the maximum curvature changes are relatively small, i.e. not exceeding 0.15 m^{-1} and 0.4 m^{-1} for the 90-direction and 0-direction, respectively. The non-linearity almost disappears when the width of the specimen is reduced, see Fig. 18, as the mid-plane stretching constraint is relaxed.

Fitting approximate best-fit straight lines to the results in Fig. 18, we obtain the following curvature-temperature relationships:

$$\Delta\kappa_0 = 1.30/150\ \Delta T = 8.7 \times 10^{-3}\Delta T$$
$$\Delta\kappa_{90} = 0.45/150\ \Delta T = 3 \times 10^{-3}\Delta T$$

here the curvature changes are in m^{-1} and the temperature changes in °C.

Note that the above estimates are about four times larger than the initial slopes in Fig. 17. The difference in resin content may be responsible for part of this discrepancy.

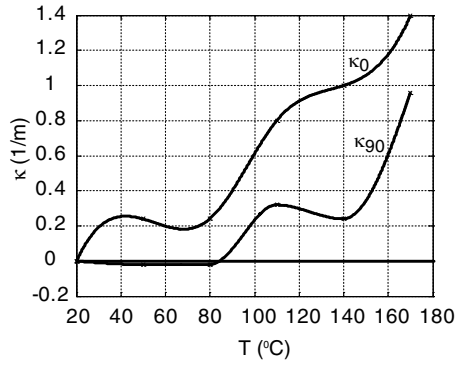

Figure 18. κ versus temperature for 30 mm wide specimens.

7. CONCLUSION

In this paper we have presented a number of experimental results and relatively simple numerical models which have allowed us to capture many features of the observed behaviour of single-ply TWF. Many of the observations presented in this paper, such as the thermal buckling observed in Section 6.3, are novel and were made very recently.

We plan to discuss in more detail our results, in the context of the existing literature, in a future publication.

Finally, we note that the samples that have been tested in the present study are rather resin rich, and so the average matrix volume fraction was 48%. In a high-quality material this value is as low as 32%, and hence the stiffness and CTE values that have been obtained should not be regarded as fully typical.

ACKNOWLEDGMENTS

AK thanks Universiti Teknologi Malaysia for financial support. This research has been partially supported by ESA-ESTEC. We are grateful to Professor H. Baier and Dr L. Datashvili for assistance with the thermal expansion measurements, Mr R. Sakai of Sakase Adtech for providing the material SK-802 and extensive information on it, Mr J. Ellis of Hexcel, Duxford for support in the preparation of specimens. We thank Professor R.M. Christensen, Dr J. Santiago-Prowald, and Dr M. Sutcliffe for helpful comments.

REFERENCES

[1] Daniel I.M., Ishai O., 1994, Engineering Mechanics of Composite Materials, Oxford University Press.

[2] Whitney J.M., Daniel I.M., Pipes R.B., 1984, Experimental Mechanics of Reinforced Composite Materials, Society for Experimental Mechanics.

[3] Kueh A., 2004, The Mechanical Properties of Triaxial Woven Fabric Composites, First-year Report, Department of Engineering, University of Cambridge.